THIEME
OPEN ACCESS

Towards the Tetrabenzo-Fused Circumazulene via In-Solution and On-Surface Synthesis

Fupeng Wu[#][a][b]
Wangwei Xu[#][c]
Yubin Fu[a][b]
Renxiang Liu[b]
Lin Yang[a][b]
Pascal Ruffieux[*][c]
Roman Fasel[c]
Ji Ma[*][a][b]
Xinliang Feng[*][a][b]

[a] Max Planck Institute of Microstructure Physics, Weinberg 2, 06120 Halle, Germany

[b] Center for Advancing Electronics Dresden (cfaed) & Faculty of Chemistry and Food Chemistry, Technische Universität Dresden, Mommsenstrasse 4, 01062 Dresden, Germany

[c] Empa – Swiss Federal Laboratories for Materials Science and Technology, 8600 Dübendorf, Switzerland

[*] pascal.ruffieux@empa.ch; ji.ma@mpi-halle.mpg.de; xinliang.feng@tu-dresden.de

[#] These authors contributed equally to this work.
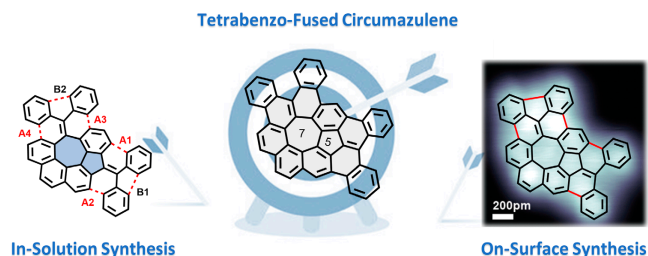
Tetrabenzo-Fused Circumazulene

In-Solution Synthesis   On-Surface Synthesis

Abstract   The synthesis of circumazulene, a nonalternant isomer of circumnaphthalene, and its π-expanded derivatives poses a considerable challenge due to the lack of a suitable synthetic strategy. In this work, we present our efforts toward achieving tetrabenzo-fused circumazulene (**1**) through both solution and on-surface syntheses. In the case of in-solution synthesis, we obtained a product (**P**) with the desired target mass, but the structural verification proved to be challenging owing to the presence of various structural isomers. In the on-surface synthesis approach, a series of unexpected azulene-embedded nanographenes were obtained, including a molecule with an additional pentagonal ring (**U1**) based on the backbone of **1**. Furthermore, theoretical calculations were conducted to shed light on these unexpected structures and to investigate their aromaticity. This work opens a new avenue for the design and synthesis of novel nonalternant graphene nanostructures incorporating circumarene.
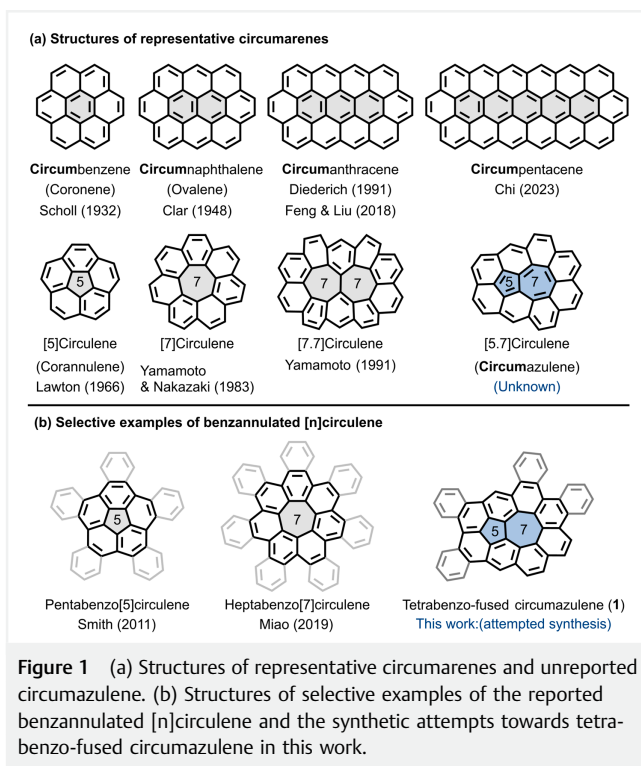
Key words: circumazulene, nanographenes, nonalternant, benzannulation, in-solution synthesis, on-surface synthesis

Introduction

Circumarenes, a unique class of nanographenes (NGs) characterized by a distinctive zig-zag edge, feature a central aromatic core surrounded by one outer layer of fused benzenoid rings.[1–3] Among these, circumbenzene (coronene)[4–8] and circumnaphthalene (ovalene)[9] (Figure 1a) stand as the smallest circumarenes, synthesized by Scholl and Clar, respectively, in the 20th century. Subsequently, their soluble derivatives were later employed in supramolecular self-assembly and electronic device applications.[10–12] Expanding upon this, a larger circumanthracene was further synthesized by Diederich et al.[13] and recently we reported its derivatives via the controlled Diels–Alder reactions of peri-tetracene.[14] Very recently, Chi et al. reported the synthesis of the largest circumarene molecule, circumpentacene, which displayed the open-shell singlet diradical character.[15]

Apart from the size expansion, the introduction of non-hexagonal rings in circumarene systems has also gained popularity due to their distinct electronic and structural features in comparison with their benzenoid counterparts.[16–21] The replacement of hexagons in circumarenes with pentagon, heptagon, or joined non-hexagonal rings (i.e., azulene or heptalene) leads to local changes in strain, dipole, and molecular symmetry, which has a significant impact on their geometries and chemical, electronic, mechanical, and magnetic properties.[22,23] For example, [5]circulene and [7]circulenes have the shape of a bowl (positive curvature) and saddle (negative curvature), respectively. Moreover, [7,7]circulene, containing a heptalene unit (two jointed heptagons), was also synthesized by Yamamoto in 1991, which has a distinctive 8-shaped geometry.[23d] In contrast, [5,7]circulene (namely, circumazulene), another important member among non-hexagonal ring-embedded circumar-

Figure 1 (a) Structures of representative circumarenes and unreported circumazulene. (b) Structures of selective examples of the reported benzannulated [n]circulene and the synthetic attempts towards tetra-benzo-fused circumazulene in this work.
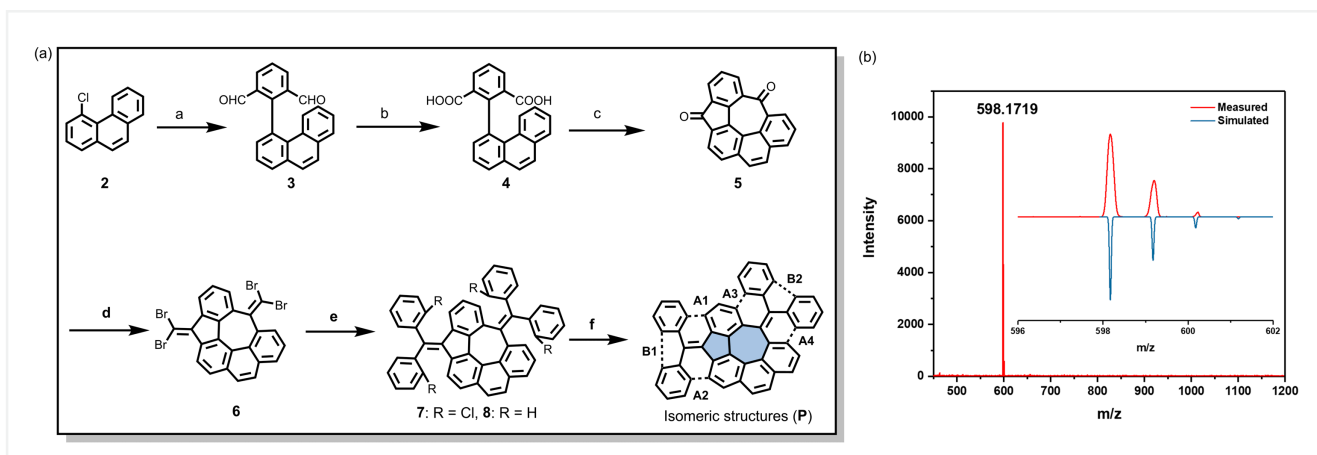
enes and serving as the nonalternant isomer of circumnaphthalene, has remained elusive. Despite its theoretical importance,[24–26] the lack of suitable synthetic methods toward circumazulene and its expanded derivatives has hindered its realization.

Herein, we report our endeavors towards the synthesis of tetrabenzo-fused circumazulene (**1**) (Figure 1b), where the benzannulation strategy is employed to expand the circumazulene with defined curvature and to further tune its chemical and electronic properties.[27–32] Our synthetic approaches include both solution-based and on-surface synthesis routes, utilizing predesigned precursors based on the indeno[6,7,1,2-*ghij*]pleiadene core.[33,34] In the context of in-solution synthesis, we successfully achieved a structure in an isomeric form with the correct molecular weight. Unfortunately, this isomeric structure, while potentially containing our target, poses challenges in terms of purification. For on-surface synthesis, a series of unexpected azulene-embedded NGs were found after the cyclodehydrogenation reaction. Interestingly, we observed the presence of a tetra-benzo-fused circumazulene analogue (**U1**), featuring an additional C–C bond that forms an extra pentagonal ring. Furthermore, the geometric, electronic structures and aromaticity of the obtained NGs have been thoroughly investigated by density functional theory (DFT) calculations.

Results and Discussion

First, the in-solution synthesis of tetrabenzo-circumazulene (**1**) from precursors **7** and **8** via Heck coupling or Scholl reaction was attempted, respectively. As shown in Scheme 1a, 4-chlorophenanthrene (**2**) was first synthesized through multi-step procedures in our previous work.[32,33] Subsequently, Suzuki coupling of compound **2** with 2-(4,4,5,5-tetramethyl-1,3,2-dioxaborolan-2-yl)isophthalaldehyde gave 2-(phenanthren-4-yl)isophthalaldehyde (**3**) in 34% yield. Then, the oxidation of dialdehyde **3** by potassium permanganate (KMnO$_4$) gave the 2-(phenanthren-4-yl)isophthalic acid (**4**) in a quantitative yield. After that, the cyclization of **4** by treatment with methanesulfonic acid (MsOH) afforded indeno[6,7,1,2-*ghij*]pleiadene-1,5-dione (**5**) with a yield of 30%. Then 1,5-bis(dibromomethylene)-1,5-dihydroindeno[6,7,1,2-*ghij*]pleiadene (**6**) was obtained from diketone **5** in a Corey–Fuchs reaction with a yield of 30%. Then, the Suzuki coupling of **6** with (2-chlorophenyl)boronic acid gave precursor **7** with a yield of 67%. The ^{1}H NMR spectrum of **7** showed broad peaks in the aromatic region likely because the rotation of the chlorinated phenyl rings is restricted by steric hindrance. Finally, the intramolecular cyclization of **7** was then carried out in dimethylacetamide (DMAc) for 12 hours in the presence of dichlorobis(tricyclohexylphosphine)palladium(II) (Pd(PCy$_3$)$_2$Cl$_2$) and a stoichiometric amount of 1,8-diazabicyclo[5.4.0]undec-7-ene (DBU). The MALDI-TOF mass spectra of the obtained product (**P**) show only one dominant peak with the expected signal at $m/z = 598.1719$ and the isotopic distribution pattern is in agreement with the simulation of the target **1**, where four bonds (A1, A2, A3, and A4) are formed according to Scheme 1b. However, the ^{1}H NMR spectrum of **P** appears complex, possibly indicating the existence of isomeric structures. We assumed that, in the cyclization via Heck reaction, various isomeric products could arise. For instance, bonds A1–A4 might only have three bonds formed, and either bond B1 or B2 could be closed to form a pentagonal ring. These isomers share the same molecular weight as target **1**, as also seen Figure S23. Despite substantial efforts, attempts to purify and grow single crystals toward the desired target **1** were unsuccessful. Scanning tunneling microscopy (STM) characterization of compound **P** was performed for structural verification. However, from the STM images, we could found two kinds of products (**P1** and **P2**) with one more bond fused than **P**, which may be due to the high temperature annealing (Figures S4 and S5).

Similar to the synthesis of tetrachloro-based precursor **7**, Suzuki coupling of **6** with the commercially available phenylboronic acid gave **8** with a yield of 57%. The structure was confirmed by NMR and HR-MALDI-TOF mass spectra (Figures S24–S26). With precursor **8** at hand, we also tested the cyclodehydrogenation in solution to synthesize targeted compound **1**. However, the initial attempt to conduct the

Scheme 1 (a) Synthetic routes toward tetrabenzo-circumazulene (**1**) via in-solution synthesis. Reagents and conditions: (a) 2-(4,4,5,5-tetramethyl-1,3,2-dioxaborolan-2-yl)isophthalaldehyde, Pd(OAc)$_2$, SPhos, K$_3$PO$_4$, toluene/EtOH/H$_2$O, 80 °C, 40 h, 34%. (b) KMnO$_4$, acetone/H$_2$O, rt, quant. (c) MsOH, 60 °C, 6 h, 30%. (d) CBr$_4$, P(OiPr)$_3$, toluene, 80 °C, 16 h, 30%. (e) For compound **7**, (2-chlorophenyl)boronic acid, Pd(PPh$_3$)$_4$, K$_2$CO$_3$, Tol/EtOH/H$_2$O, 85 °C, 24 h, 67%; for compound **8**, phenylboronic acid, Pd(PPh$_3$)$_4$, K$_2$CO$_3$, toluene/EtOH/H$_2$O, 85 °C, 24 h, 57%. (f) Heck reaction of compound **7**, Pd(PCy$_3$)$_2$Cl$_2$, DBU, microwave, 150 °C, 12 h; the Scholl reaction of compound **8**, DDQ/TfOH, CH$_2$Cl$_2$, rt. 1 h. (b) HR MALDI-TOF MS spectrum of the achieved isomeric structures (**P**). Inset: experimental (red solid line) and simulated (blue solid line) isotopic distribution patterns of the mass peak.

Scholl reaction of precursor **8** utilizing DDQ/TfOH only yielded partially cyclized products (Figure S3).

Additionally, theoretical calculations on **1** were carried out at the B3LYP/6–31 G(d) levels in comparison with circumazulene to gain insights into the difference in their geometries and electronic structures. After the benzannulation, **1** exhibits slightly elevated energy levels for both the highest occupied molecular orbital (HOMO; −5.02 eV) and lowest unoccupied molecular orbital (LUMO; −2.14 eV) energy lev-els compared to circumazulene (HOMO: −5.08 eV, LUMO: −2.19 eV) (Figure S10). Most of the HOMO of **1** is located around the heptagonal rings, while the LUMO is distributed mostly around the pentagonal rings (Figure 2c, d). Furthermore, the geometry of circumazulene undergoes a transformation from a planar to a curved configuration in **1** after benzannulation with four benzene rings (Figure S10). The optoelectronic properties of the obtained product **P** were investigated with UV-vis-NIR spectroscopy. As shown in

Figure 2 DFT calculation of **1** at the B3LYP-6–31 G(d) level: optimized structure (a) top view; (b) side view; (c) LUMO, and (d) HOMO and values of their energy level. (e) UV-vis absorptions of **P** measured in dichloromethane (9.47 M^{-1}) at 298 K.
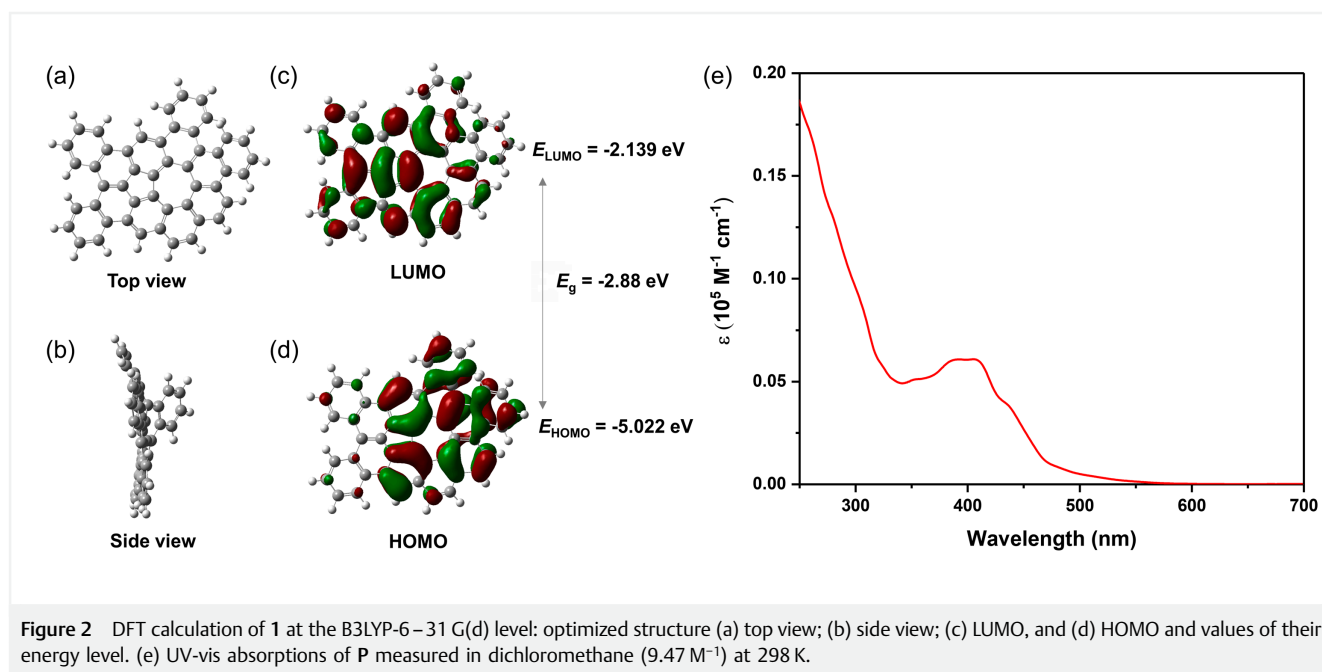
Figure 2e, the mixture product exhibited a broad absorption band with the maximum absorption wavelength (λ_{max}) at 405 nm. In addition, the optical energy gap (E_g^{opt}) of **P** was estimated to be 2.26 eV from the onset wavelength of its UV-vis absorption.

Due to the unsuccessful attempts at in-solution synthesis, we redirected our efforts toward the on-surface synthesis of tetrabenzo-circumazulene (**1**) from precursors **7** and **8**. Precursor **7** or **8** was deposited on the Au (111) surface and annealed to high temperature to promote oxidative cyclization toward **1**.

Firstly, precursor **8** was deposited on the Au (111) surface at room temperature, where the majority of the molecules cluster together and only a few single molecules remain (Figure S6a). After that, **8** was annealed at 250 °C and 330 °C on Au (111), with their corresponding STM images displayed in Figure S6. Contrary to expectations, no targeted product **1** was found after annealing **8** on Au (111) at 330 °C for 15 minutes (Figure 3). Instead, unexpected cyclization products **U1, U2**, and **U3** were observed (Figure 3d – f). However, the yield of these three products was low, and only a few molecules have been observed. Beyond our expectations, most of the precursor molecules lost a diphenylmethane unit on the pentagon ring side, and a new monomeric product (**M1**) was found (Figure 3a, b). In addition, another side product (**M2**)

was also found (Figure 3a, c). Compound **M2** lost 14 carbon atoms compared to **M1**, possibly due to a rearrangement, but we lack insight into the reaction pathway at this point. In addition, the dimerization products **D1** and **D2** were formed (Figure S7). The formation of **D1** comes from the dimerization of **M1**, while **D2** arises from the dimerization of compounds **M1** and **M2**. In addition, no Kondo resonance peak was found in **M1**, suggesting the existence of a CH$_2$ group on the pentagonal ring.

For comparison, compound **7** was also subjected to on-surface experiments. However, after annealing at 330 °C, our attempts to obtain the targeted compound **1** were unsuccessful (Figures S8 and S9). Instead, we observed only unexpected products (**U1**–**U3**), which were similarly noted during on-surface synthesis using precursor **8**.

In order to elucidate their formation mechanisms and provide insights into the differences in their aromaticity, we performed theoretical calculations on circumazulene, compound **1**, and three unexpected products (**U1**–**U3**) at the B3LYP/6 – 31 G(d) levels. According to the calculation results, the optimized structure of the desired target **1** demonstrates a more pronounced curvature (Figure S10). The significantly increased strain arising from the curved structure poses challenges in the on-surface synthesis of **1**, resulting in unexpected molecules (**U1**–**U3**), all of which exhibit more
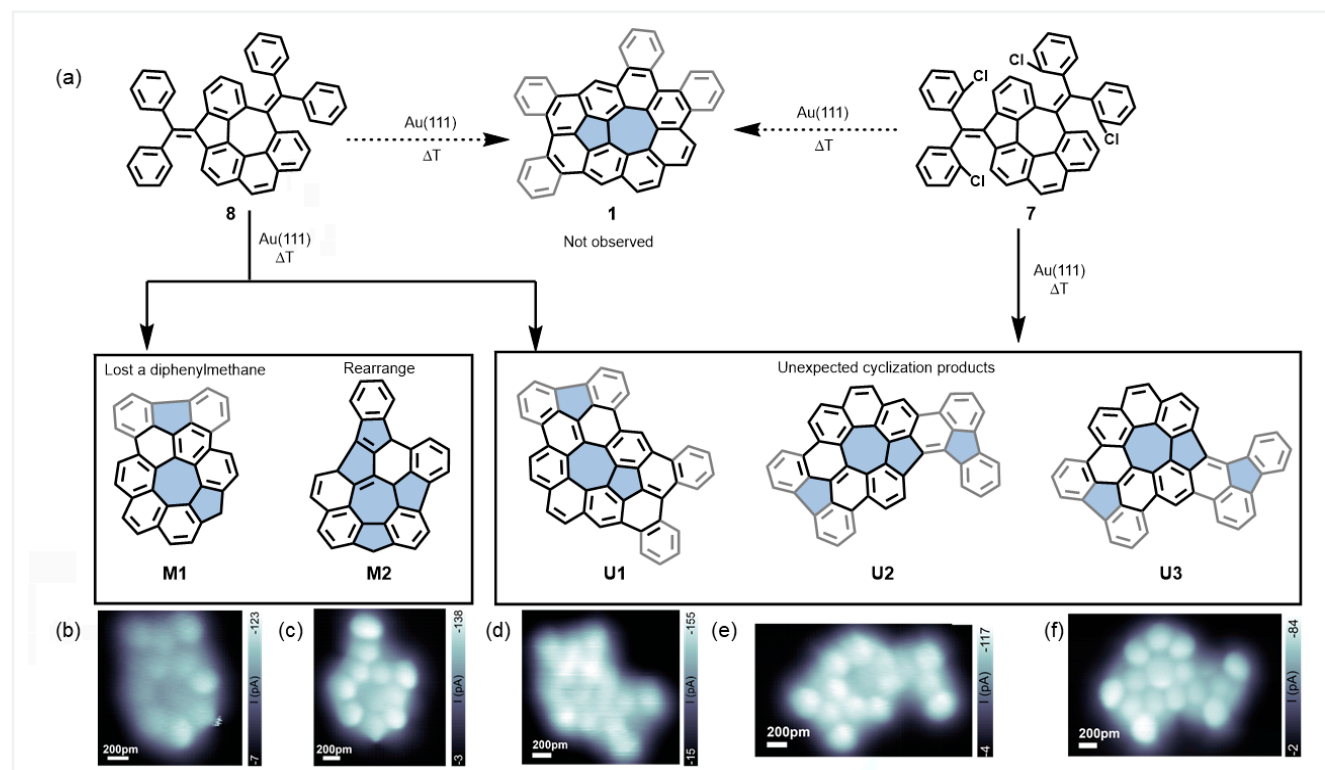

Figure 3 (a) On-surface synthesis of tetrabenzo-circumazulene (**1**) from precursor **7** and **8**. UHR STM images of some unexpected products after annealing precursor **7** or **8** on Au (111) at 330 °C for 15 min. (b) **M1**, (c) **M2**, (d) **U1**, (e) **U2**, (f) **U3**. Scanning parameter: bias voltage −5 mV.
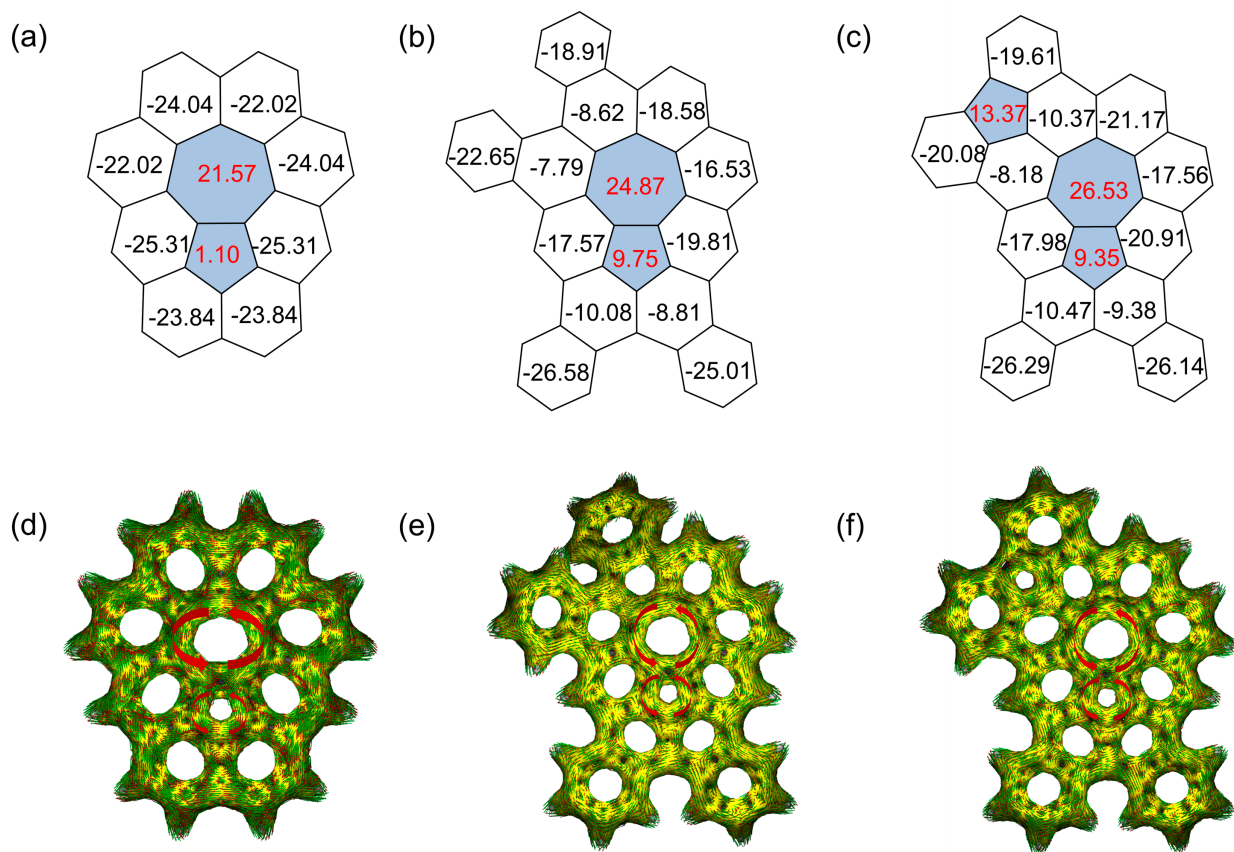
Figure 4   (a – c) NICS(1)$_{zz}$ values and (d – f) ACID plots of circumazulene, tetrabenzo-circumazulene (**1**) and unexpected on-surface synthesis product (**U1**), respectively. The non-hexagonal rings are highlighted in blue color.

planar structures (Figure S10). To further analyze the aromaticity of circumazulene, **1** and **U1**, nucleus-independent chemical shift (NICS)[35] and anisotropy of the induced current density (ACID)[36,37] calculations at the B3LYP/6 – 311+G (d,2 p) level of theory were performed. In these three molecules, all the NICS(1)$_{zz}$ values of hexagonal rings are negative, indicative of their aromatic character, while the values of pentagonal and heptagonal rings are positive, suggesting the antiaromatic character for the non-benzenoid rings (Figure 4a – c). In addition, the NICS(1)$_{zz}$ values of heptagons are notably larger than that of pentagons, implying a stronger antiaromatic character for the heptagonal rings. Interestingly, the NICS(1)$_{zz}$ values increase from circumazulene to **1** to **U1**, going from 21.57 to 24.87 and 26.53. This trend indicates that the heptagonal ring in **U1** possesses the strongest antiaromatic character. Moreover, all pentagonal rings also show small positive NICS(1)$_{zz}$ values, suggesting their weak antiaromatic character. This antiaromatic character of non-benzenoid rings is not like that of the azulene, in which both pentagonal and heptagonal rings show aromatic character. These results are further supported by the anticlock-

wise ring current flow in the non-benzenoid rings and the diatropic ring current circuits in the peripheral benzene rings as shown in ACID maps (Figure 4d – f and Figures S11 – S13).

Conclusions

In summary, we detail our endeavors toward the synthesis of tetrabenzo-fused circumazulene (**1**), which can be viewed as the benzannulation of four benzene rings with a circumazulene core. Two synthetic strategies including in-solution and on-surface synthesis were conducted. In the in-solution approach, the product obtained through the Heck reaction of **7** displayed the correct molecule weight of **1**, but the structural verification proved challenging due to the presence of various isomers. On the other hand, on-surface synthesis from either **7** or **8** resulted in a series of unexpected azulene-embedded NGs, failing to yield the target structure of **1**. It is worth mentioning that an unexpected product (**U1**) featuring an additional pentagonal ring was obtained, incor-

porating the core of tetrabenzo-circumazulene. Theoretical calculations of the studied azulene-embedded NGs indicated the strong antiaromatic character of the inner non-benzenoid rings, particularly heptagonal rings. This is different from the normal azulene, in which both pentagonal and heptagonal rings show aromatic character. This exploration paves the way for the synthesis of novel graphene nanostructures containing circumarenes, such as circumazulene or its benzo-extended derivatives.

Funding Information

Acknowledgment

Supporting Information

Supporting Information for this article is available online at https://doi.org/10.1055/a-2333-9789.

Conflict of Interest

The authors declare no conflict of interest.

References and Notes

(1) Zou, Y.; Hou, X.; Wei, H.; Shao, J.; Jiang, Q.; Ren, L.; Wu, J. *Angew. Chem. Int. Ed.* **2023**, *62*, e202301041; *Angew. Chem.* **2023**, *135*, e202301041.

(2) Liu, J.; Feng, X. *Angew. Chem. Int. Ed.* **2020**, *59*, 23386; *Angew. Chem.* **2020**, *132*, 23591.

(3) Chen, Q.; Schollmeyer, D.; Müllen, K.; Narita, A. *J. Am. Chem. Soc.* **2019**, *141*, 19994.

(4) Newman, M. S. *J. Am. Chem. Soc.* **1940**, *62*, 1683.

(5) Craig, J. T.; Halton, B.; Lo, S. *Aust. J. Chem.* **1975**, *28*, 913.

(6) Shen, H.-C.; Tang, J.-M.; Chang, H.-K.; Yang, C.-W.; Liu, R.-S. *J. Org. Chem.* **2005**, *70*, 10113.

(7) Van Dijk, J. T.; Hartwijk, A.; Bleeker, A. C.; Lugtenburg, J.; Cornelisse, J. *J. Org. Chem.* **1996**, *61*, 1136.

(8) Scholl, R.; Meyer, K. *Ber. Dtsch. Chem. Ges.* **1932**, *65*, 902.

(9) Clar, E. *Nature* **1948**, *161*, 238.

(10) Rohr, U.; Schlichting, P.; Böhm, A.; Gross, M.; Meerholz, K.; Bräuchle, C.; Müllen, K. *Angew. Chem. Int. Ed.* **1998**, *37*, 1434.

(11) Saïdi-Besbes, S.; Grelet, É.; Bock, H. *Angew. Chem. Int. Ed.* **2006**, *45*, 1783.

(12) Li, J.; Chang, J.-J.; Tan, H. S.; Jiang, H.; Chen, X.; Chen, Z.; Zhang, J.; Wu, J. *Chem. Sci.* **2012**, *3*, 846.

(13) Broene, R. D.; Diederich, F. *Tetrahedron Lett.* **1991**, *32*, 5227.

(14) Ajayakumar, M.; Fu, Y.; Ma, J.; Hennersdorf, F.; Komber, H.; Weigand, J. J.; Alfonsov, A.; Popov, A. A.; Berger, R.; Liu, J. *J. Am. Chem. Soc.* **2018**, *140*, 6240.

(15) Jiang, Q.; Wei, H.; Hou, X.; Chi, C. *Angew. Chem. Int. Ed.* **2023**, *62*, e202306938; *Angew. Chem.* **2023**, *135*, e202306938.

(16) Balaban, A. T.; Randić, M. *J. Chem. Inf. Comput.* **2004**, *44*, 1701.

(17) Márquez, I. R.; Castro-Fernández, S.; Millán, A.; Campaña, A. G. *Chem. Commun.* **2018**, *54*, 6705.

(18) Miyoshi, H.; Nobusue, S.; Shimizu, A.; Tobe, Y. *Chem. Soc. Rev.* **2015**, *44*, 6560.

(19) Pun, S. H.; Miao, Q. *Acc. Chem. Res.* **2018**, *51*, 1630.

(20) Tobe, Y. *Chem. Rec.* **2015**, *15*, 86.

(21) Fei, Y.; Liu, J. *Adv. Sci.* **2022**, *9*, 2201000.

(22) Butterfield, A. M.; Gilomen, B.; Siegel, J. S. *Org. Process Res. Dev.* **2012**, *16*, 664.

(23) (a) Feng, C.-N.; Kuo, M.-Y.; Wu, Y.-T. *Angew. Chem. Int. Ed.* **2013**, *52*, 7791. (b) Barth, W. E.; Lawton, R. G. *J. Am. Chem. Soc.* **1966**, *88*, 380. (c) Yamamoto, K.; Harada, T.; Nakazaki, M.; Naka, T.; Kai, Y.; Harada, S.; Kasai, N. *J. Am. Chem. Soc.* **1983**, *105*, 7171. (d) Yamamoto, K.; Saitho, Y.; Iwaki, D.; Ooka, T. *Angew. Chem. Int. Ed. Engl.* **1991**, *30*, 1173.

(24) Banhart, F.; Kotakoski, J.; Krasheninnikov, A. V. *ACS Nano* **2011**, *5*, 26.

(25) (a) Müllen, K. *Nat. Rev. Mater.* **2016**, *1*, 1. (b) Rasool, H. I.; Ophus, C.; Zettl, A. *Adv. Mater.* **2015**, *27*, 5771.

(26) Pun, S. H.; Wang, Y.; Chu, M.; Chan, C. K.; Li, Y.; Liu, Z.; Miao, Q. *J. Am. Chem. Soc.* **2019**, *141*, 9680.

(27) Reisch, H. A.; Bratcher, M. S.; Scott, L. T. *Org. Lett.* **2000**, *2*, 1427.

(28) Wu, J.; Pisula, W.; Müllen, K. *Chem. Rev.* **2007**, *107*, 718.

(29) Stabel, A.; Herwig, P.; Müllen, K.; Rabe, J. P. *Angew Chem. Int. Ed. Engl.* **1995**, *34*, 1609.

(30) Miller, R. W.; Duncan, A. K.; Schneebeli, S. T.; Gray, D. L.; Whalley, A. C. *Chem. Eur. J.* **2014**, *20*, 3705.

(31) Sakamoto, Y.; Suzuki, T. *J. Am. Chem. Soc.* **2013**, *135*, 14074.

(32) Xiao, S.; Myers, M.; Miao, Q.; Sanaur, S.; Pang, K.; Steigerwald, M. L.; Nuckolls, C. *Angew. Chem. Int. Ed.* **2005**, *44*, 7390.

(33) Wu, F.; Ma, J.; Lombardi, F.; Fu, Y.; Liu, F.; Huang, Z.; Liu, R.; Komber, H.; Alexandropoulos, D. I.; Dmitrieva, E. *Angew. Chem. Int. Ed.* **2022**, *61*, e202202170; *Angew. Chem.* **2022**, *134*, e202202170.

(34) Wu, F.; Barragán, A.; Gallardo, A.; Yang, L.; Biswas, K.; Écija, D.; Mendieta-Moreno, J. I.; Urgel, J. I.; Ma, J.; Feng, X. *Chem. Eur. J.* **2023**, *29*, e202301739.

(35) Schleyer, P. V.; Maerker, C.; Dransfeld, A.; Jiao, H. J.; Hommes, N. *J. Am. Chem. Soc.* **1996**, *118*, 6317.

(36) Herges, R.; Geuenich, D. *J. Phys. Chem. A* **2001**, *105*, 3214.

(37) The UV-visible spectra were measured on an Agilent Cary 5000 UV-VIS-NIR spectrophotometer. All density functional theory calculations were performed using the Gaussian 09 program. The geometry optimization of all the study compounds in the ground state was optimized by the B3LYP/6–31 G(d). STM measurements and on-surface synthesis were performed with commercial Scienta Omicron low-temperature

STM operating at base pressure below 1×10^{-10} mbar. UHR STM images were acquired by recording the current channel while scanning the molecules in constant-height mode with CO-functionalized tips. The STM images were analyzed using Igor. Detail information about the general procedure as well as the analytical data of compounds/materials is provided in the Supporting Information.